DOI: 10.13009/EUCASS2019-258

Fragmentation and formation of the condensed products during combustion of titanium particles in air

Belousova N. S., Glotov O. G.**, Surodin G. S.****

** Voevodsky Institute of Chemical Kinetics and Combustion, Siberian Branch of the Russian Academy of Sciences, 630090, Institutskaya str., 3, Novosibirsk, Russia*

Novosibirsk State Technical University, 630073, Karl Marx ave., 20, Novosibirsk, Russia

nata.bel.94@mail.ru

*** Voevodsky Institute of Chemical Kinetics and Combustion, Siberian Branch of the Russian Academy of Sciences, 630090, Institutskaya str., 3, Novosibirsk, Russia*

Novosibirsk State Technical University, 630073, Karl Marx ave., 20, Novosibirsk, Russia

glotov@kinetics.nsc.ru

**** Voevodsky Institute of Chemical Kinetics and Combustion, Siberian Branch of the Russian Academy of Sciences, 630090, Institutskaya str., 3, Novosibirsk, Russia*

surodin@kinetics.nsc.ru

Abstract

The Ti particles combustion in air mechanism was investigated aiming to increase the efficiency of initial particles transformation into oxide products. This study was focused on the fragmentation process features and the condensed combustion product particles characteristics. It was found that in combustion of each coarse particle the final coarse oxide residue particle forms along with highly dispersed oxide smoke. The coarse particle formation is due to specific so-called "fir branch" fragmentation regime. In combustion of fine Ti particle the different "star burst" fragmentation regime is executed that is preferable for the highly dispersed oxide formation.

1. Introduction

One of the reasons for today's interest in titanium particle combustion is the prospect of using metallic titanium in technological combustion, aimed at producing nanosized titanium dioxide [1]. Titanium particles can be burnt in the form of air suspensions [2, 3], and aerogels [4, 5] either in a dust torch [6] or in a composite system, including titanium, oxidizer, and binder [7]. It turned out, however, that in the combustion wave of the such kind composite system, including solid oxidizer, polymeric binder, and powdered titanium with a particle size on the order of units-tens of micrometers, the agglomeration of metal occurs [1, 7]. As a result, the agglomerates leaving the burning surface, are sized of the hundreds of micrometers rather than the initial micrometer titanium particles. This has inspired studies on the combustion first of large ($D > 300$ μm) titanium agglomerates [8–11], and then of large monolithic Ti particles [12, 13] in air. A new fragmentation regime, called the "fir-tree branch", or simply "fir branch" was revealed for large agglomerates and monolithic particles. As compared to the well-known regime with a single star-type explosion of a mother particle (the so-called "star burst" or simply "star" regime), a new fragmentation regime is realized as a prolonged, continuous shooting of many small particles-fragments from the mother particle with its further conservation. When combustion is over, the mother particle residue is represented by a large oxide particle comparable in size with the mother one. No similar residues have been observed for fragmentation performed in the "star" regime. Obviously, the phenomenon of fragmentation can reduce burning time and favours the effective transformation of initial metal into highly disperse oxide products. In this case, the "star" regime is preferable due to the absence of the large, final oxide particle-residue. Therefore, the works [12, 13] were devoted to the determination of combustion times and conditions for the change in fragmentation regime "fir branch" ⇔ "star". For the monolithic particles with a diameter of 120 – 540 μm, we determined the dependence of burning times on particle diameter as $t_b(D) = 3.53\times10^{-6}\cdot D^{2.05}$, where t_b is in [s], and D is in [μm]. The limiting diameter of particles, at which the fragmentation regimes change, amounts to 250 – 300 μm. We revealed and described the main morphological types of particles – combustion products. This work continues the studies performed in [12, 13] and presents a quantitative characterization of the combustion product particles and the fragmentation of mother particle.

DOI: 10.13009/EUCASS2019-258

2. Performing and processing experiments

In this work, experiments on particle combustion in free fall in air were carried out as described in [8, 12, 13]. The sample was represented by a strip of metal-free propellant-matrix with sizes W×L×H of about 3×25×2 mm, applied to a quartz tube of ∅12 mm. There are special cavities in the strip where metal inclusions are located. The inclusions (5-10 items in one sample) have the form of flat pieces of metal titanium of 99.38 % purity and with dimensions of about 1×1×0.06 mm. When a combustion wave passes along the propellant-matrix strip, the latter ignites and throws away the particles. In combustion, the particles acquire a spherical form, their initial diameter is determined from the geometric dimensions of inclusions as described in [12, 13]. Experiments were carried out as follows, see Figure 1.
Sample tube-holder 1 was fixed horizontally above the upper, open end of large quartz tube 2 with dimensions of ∅8.2×220 cm so that the cavities were directed downwards and the particles were ejected downwards. The lower end of the tube was placed on the Petri dish 4. The sample was ignited, and the flight of burning particles in the large tube was recorded by camera 3 at 25 frames per second. Immediately after sample combustion, the tube-holder was removed and the top end of the tube 2 was covered with a lid. The tube was left alone for a long time (from an hour to 41 days, usually for 24 h) so that the particles-products settled on the Petri dish. The bottom of the dish was covered with aluminum foil. The objects chosen could be moved under an electron microscope without touching them by cutting a corresponding foil fragment (e. g., a square of 7×7 mm) with a sharp blade. Optionally, microscope slides were placed in the dish. Video records provided the combustion times and the characteristic times at which the fragmentation started and ended. In addition, important information was extracted about the number of burning particles-sources and the character of their burning.

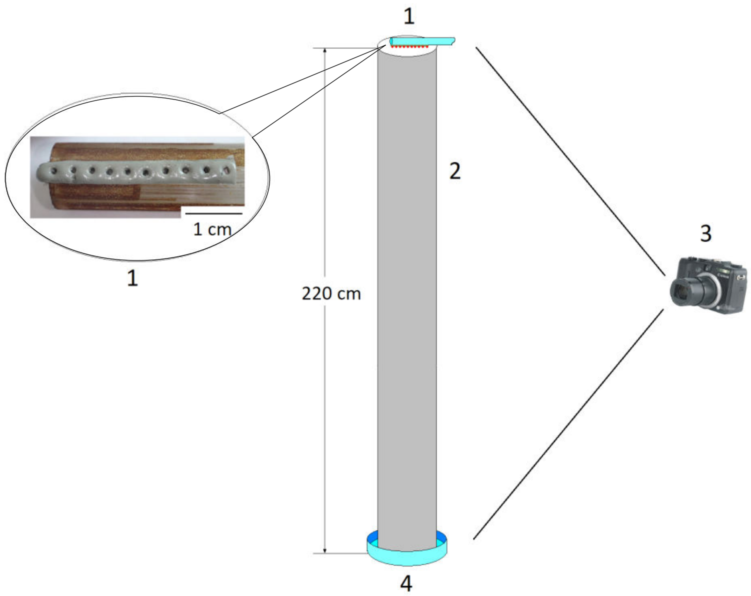

Figure 1: Experimental scheme. 1 – sample on a tube-holder, 2 – large quartz tube, 3 – camera, 4 – Petri dish

The particles sampled were subjected to morphological and granulometric analyses by optical methods with image construction. The following equipment was used: Sony DSC-TX30 camera in super magnifier mode, projection microscope with an screen image scale of 8.26 micrometer/mm, microscope MBS-10 with an ocular camera DCM-300, scanner Epson Perfection 4990 Photo with an image scale of 5.29 micrometer/pixel in 4800 DPI mode, and scanning electron microscope (SEM) Merlin|VP Compact (Zeiss) with EDS-device X-Max^{N} (Oxford Instruments) for local elemental analysis by EDS – energy dispersive spectroscopy. The images were processed with an original software. Figure 2 schematically demonstrates the processing of the Petri dish image taken with the scanner.

DOI: 10.13009/EUCASS2019-258

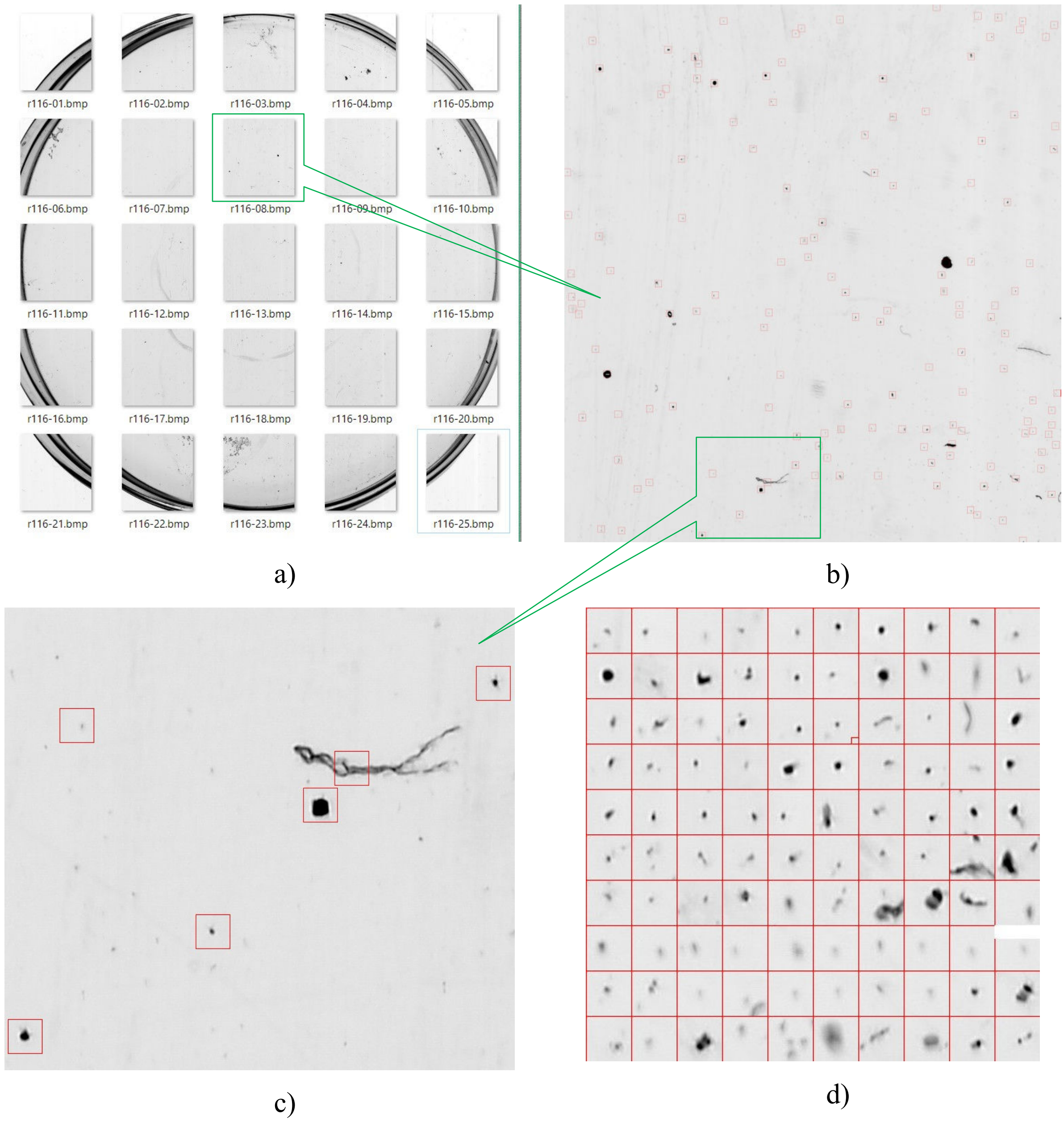

Figure 2: Application of original software for processing images of the type “very large field with rare in occurrence the object to be measured”

a) The image of the Petri dish (scanned with high-resolution) with the particles sampled is cut into 25 fields.

b) In each field, we marked the objects with a mouse button for future measurements. Then the program outlines the marked objects with red squares.

c) The enlarged fragment of the previous image demonstrates the object choice squares.

d) The squares chosen are automatically copied in a new file-mosaic.

The pixel measurements of objects are performed using these mosaics.

DOI: 10.13009/EUCASS2019-258

3. Results

In this work, we have distinguished several morphological types of combustion products. Let us describe them.

3.1 Large residues of mother particles

The large particle-residue is shown in Figure 3. Fragmentation in the “fir branch” regime during combustion of a large mother particle, results, as a rule (but not always), in a particle-residue, comparable in size with the initial mother particle. These particles are usually light yellow [9, 12, 13]. The diameter of the largest residue is typically 0.56 – 0.32 of the diameter of the mother particle and that of the next largest particle amounts to 0.23 – 0.20 of the diameter of the mother one. A purposive, mechanical destruction of large particles-residues showed that the latter are hollow. The thickness of the shell wall is different in the different sites and amounts to 10 – 30 μm for a residue diameter of about 250 μm, and of 10 – 70 μm for a diameter of about 400 μm. The EDS analysis of 14 points on the surface and inside four destroyed particles provided the following ratio of atoms O/T = 3.3 (standard deviation Sd = 1.7, standard error of mean Se = 0.4).

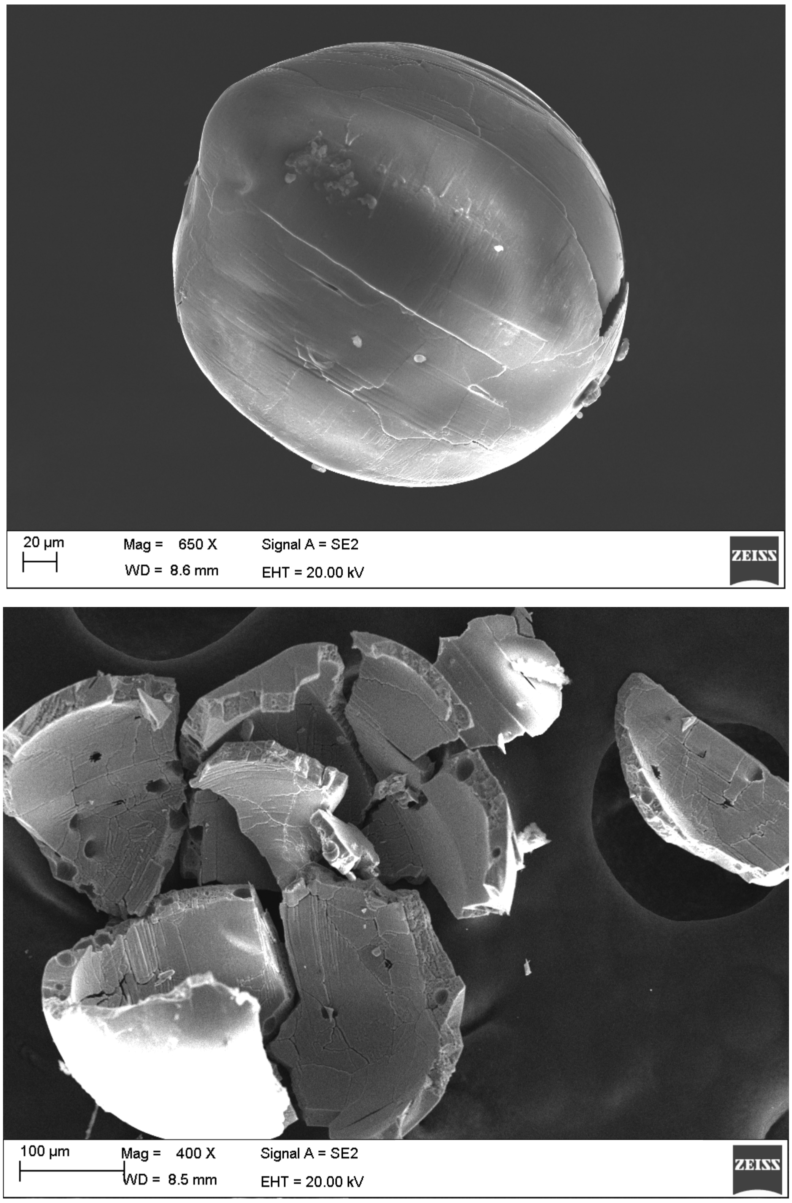

Figure 3: Typical, large particle-residue.

On top – before destruction, below – after destruction. Particle structure – gas bubble in a shell

DOI: 10.13009/EUCASS2019-258

3.2 Small spherical particles

Figure 4 shows the small, spherical particles. Unlike the large residues of mother particles, the small ones are mainly the residues of fragment combustion. There is no clear boundary between large and small residues. For example, there are cases where the mother particle fragments into 2 – 3 large fragments. In this situation, the “small” residues can have diameters on the order of hundreds of micrometers, i. e., they are close in order of magnitude to the particles, formed in cases with a single large residue. Usually, the small, spherical particles under study have the diameter on the order of units-tens of micrometers. Most of the particles are light yellow and sometimes, grey or black-violet, figure 4c. Note that oxide Ti_2O_3 is black-violet [11]. Under special lighting, some particles manifest a acorn-type structure, figure 4d, which is well known and typical of burning aluminum particles [14]. However, for titanium, the “core” is hidden under the layer of oxide and just shines through it. It is difficult to mechanically destroy small particles in order to study their inner combustion. Besides, no EDS-analysis of these particles was performed. As the particles are covered by the oxide layer, they often look “vitrified” under an optical microscope. In the case of the black-violet particles, the interference rainbow colors can be observed on the outer oxide layer. The small, spherical particles have a distributed electric charge and can jump on each other and remain in this position, figure 4a. The jumps of the particles were observed under an electron microscope. In addition, typical is the adhesion of small, spherical particles with an aggregate of nanoparticles-spherules, as shown in figure 4b.

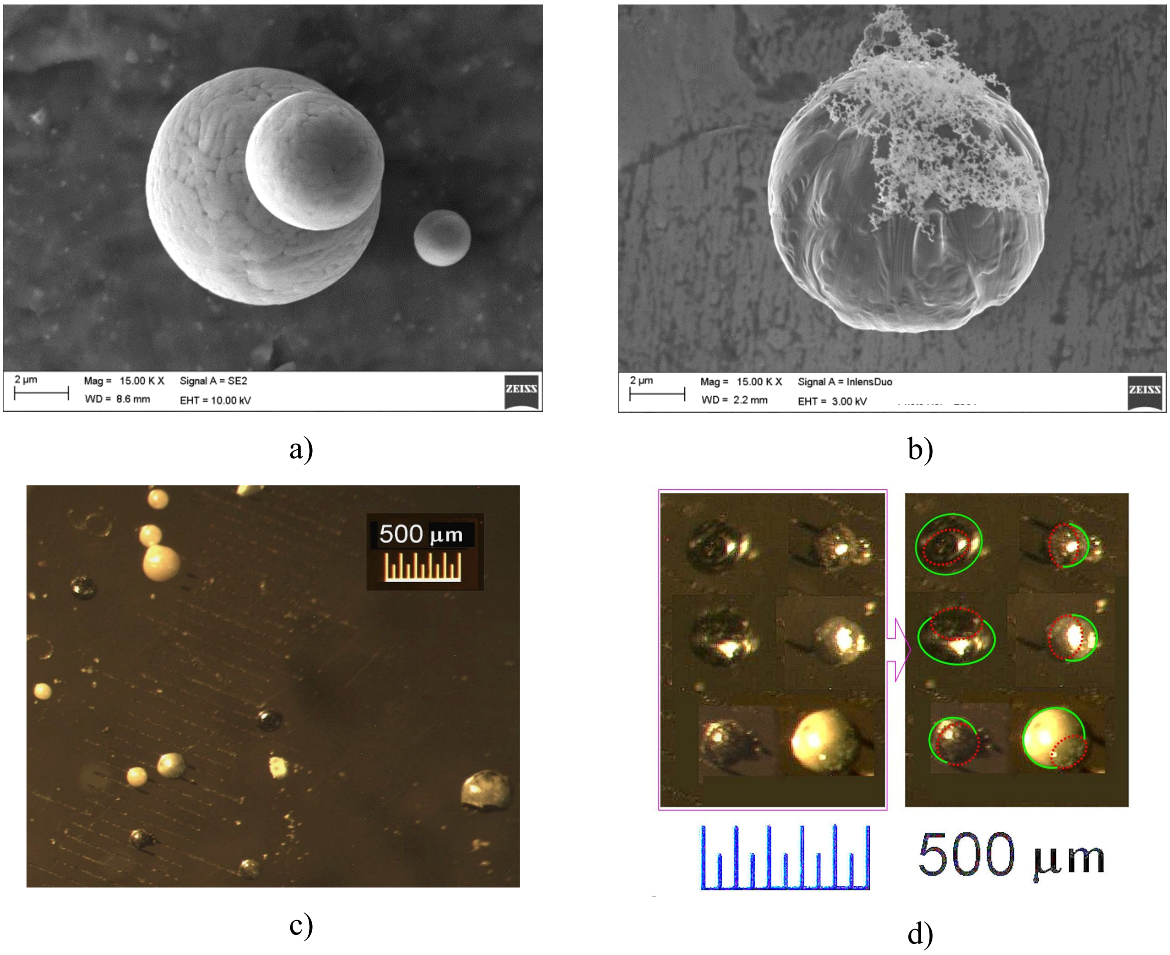

Figure 4: Small, spherical particles – fragment combustion residues.

a), b) – view under an electron microscope; demonstration of electric charges that make the particles stick together.

a) – micrometer size particles sticking together, b) – micrometer size particles sticking with a “network” of nanoparticles. c), d) – view under the optical microscope, demonstration of both the particles of various colors and their acorn structure. The right-hand part of the figure d) is identical to the left one but it denotes the core and the shell by dotted and solid lines for clarity

DOI: 10.13009/EUCASS2019-258

3.3 Aerogel objects

The aerogel objects are shown in figures 5 and 6. Remember that the aerogel objects, formed from the primary nanoparticles-spherules in a trace of a burning mother particle, have been first described in [15]. In the present work, aerogel objects are the focus of attention for two reasons. First, they represent a practical embodiment of oxide nanoparticles that can be considered as a target product of titanium combustion. Second, these objects are actually the frozen oxide smoke track and their geometric parameters reflect a temporal history of smoke formation.

In the current processing, we have distinguished the aerogels of two types, i. e., *aerogel round clouds* (ARC) and *aerogel elongated clouds* (AEC). When observed with a naked eye, the clouds are white with a bluish tinge. The name ARC reflects the method for measuring these objects rather than their real shape. The shape of ARC objects resembles a cloud (figures 5a and 5b). In this case, their size is almost the same in different directions. Thus, the ARC objects were measured by circle fitting. The AEC objects resemble tadpoles (figure 5c). These are characterized by a relatively large extent in one direction. The longest recorded object of the AEC type was 15 mm in length (figure 5e). The AEC objects were measured in two directions, recording both the length of the maximal axis and a characteristic size perpendicular to the long axis as shown in one of figures 5c. The electron microscope allows us to see that the aerogel objects consist of spherules with a diameter on the order of tens of nanometers (figure 5d). The spherules are united into chains but fail to form a dense packing. Thus, the aerogel clouds are the nanostructured macroscopic objects. The spherules were measured by circle fitting, using the images similar to that in figure 5d. In this case, we measured only the clearly visible ones within the depth of focus. It is assumed then that the objects of the ARC type result from fragmentation of fragments, i. e., in the “star explosion” regime of relatively small burning titanium particles-fragments. The objects of the AEC type are likely to arise from the fragmentation in the regime similar to the “fir branch” one typical of the particles exceeding 250 – 300 μm [12, 13]. A continuous shooting of fragments causes a prolonged ejection of nanoparticles. When moving, the particles form a characteristic trace-cloud. The number and the geometric dimensions of the AEC objects indicate that they were generated not by the primary (large) mother particles but by their fragments. The shape of the aerogel cloud stores information on the character of combustion and fragmentation. Thus, e.g., a typical tadpole-shape is realized in the cases where the particle burns with almost time-constant emission of nanoparticles and ends its life with a star explosion. As shown in figure 5e, the intensity of nanoparticle formation is not time-constant (the trace width changes periodically) and at the end of combustion the particle is divided into almost equal fragments either of which ends its life with a star explosion. The shapes of elongated clouds can be more complex, e. g., arch or spiral, see figure 6. Arch trace *1* exhibits successive explosions. This pattern is met quite often. Spiral trace *2* testifies to the rotation of a burning particle.

Trial attempt of the analysis of an object similar to shown in figure 5b with EDS method "on the area" gave a ratio of O/T atoms = 9.2. This result forces us to assume that application of the EDS method in this case is incorrect.

DOI: 10.13009/EUCASS2019-258

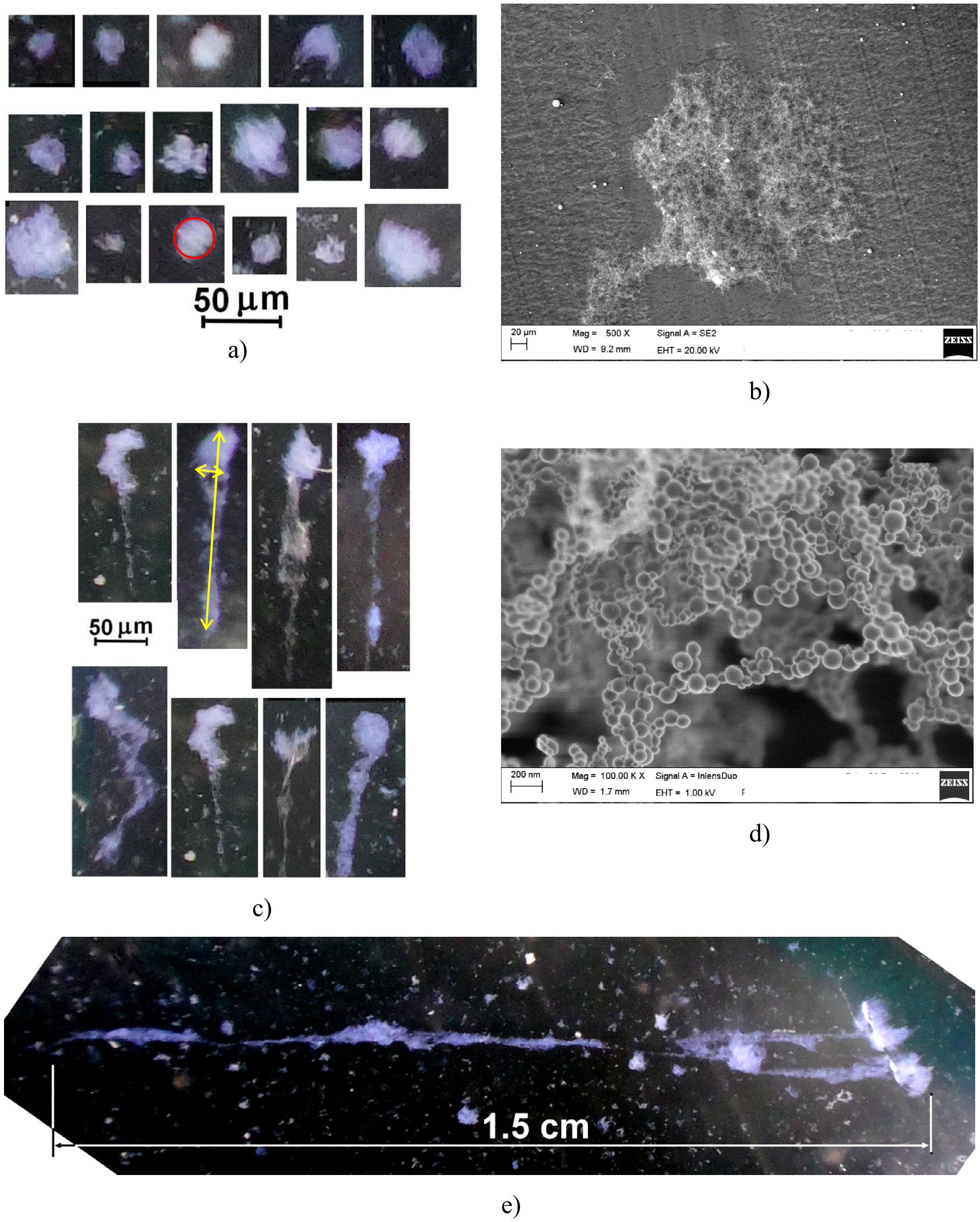

Figure 5: Aerogel objects

a), b) – «round» clouds (ARC), the view under an optical microscope on the Petri dish (a), and under an electron microscope on a substrate of aluminum foil (b).

c), e) – elongated clouds (AEC) on the Petri dish. Circle in the figure (a) and arrows in the figure (c) demonstrate the methods for measuring round and elongated objects, respectively.

d) – the structure of aerogel objects under an electron microscope. These consist of a chain of nanosized spherules.

DOI: 10.13009/EUCASS2019-258

Figure 6: Aerogel objects of unusual shape. *1* – arch trace with four explosions, *2* – spiral trace

3.4 Granulometric data

Below, exemplified is a quantitative processing of the data on the granulometric composition of the particles of the different morphological types is described. The methods of particle measurement are presented above. These results refer to the experiment with the following parameters: the number of burning mother particles – 5, their diameter range – 354 – 552 µm, and mean diameter of mother particle – 437 µm. All the particles were fragmented in the “fir branch” regime, two of five particles hit the wall of the large tube in the flight (thus their combustion can be perturbed). Figure 7 shows the counting size-distributions of the number of particles, normalized to the number of burning particles. The compact spherical particles are collected in a single histogram without distinguishing large and small residues. For the AEC objects, the cloud length was taken as their size. In this experiment, the maximal AEC was 11250 µm long. Therefore, the plot presented is the fragment of the whole distribution limited in size to 700 µm. The minimal size of the particles measured was 60 µm. For the particles smaller than 60 µm, we counted only their total number, the compact spheres and ARC, separately. In terms of one mother particle, the number of compact spheres was 8999 and that of ARC amounted to 13499. The ratio between the compact spheres and clouds of nanoparticles was 40% : 60% (± 3 %). Figure 8 demonstrates the size-distributions of spherules by number. For spherules, the distribution was not normalized and a relative frequency was plotted on the y-axis. The distribution functions in figures 7 and 8 were approximated by log-normal distributions. The table 1 summarizes the size distribution parameters.

Table 1: Parameters of approximating log-normal distributions

	Median ***xc***	**Width** ***w***	**Amplitude** ***Am***	$\mathbf{R^2}$
spheres	112±1 µm	0.28±0.01	9147±309	0.984
ARC	147±2 µm	0.19±0.01	47689±3216	0.920
AEC	367±3 µm	0.33±0.01	4999±114	0,823
spherules	48±0.4 nm	0.24±0.01	10.1±0.3	0.990

The value after ± is Se – standard error of mean.
R^2 – determination coefficient.
The log-normal distribution formula:

$$y(D) = \frac{Am}{wD\sqrt{2\pi}}\exp\left(\frac{-\left[\ln\frac{D}{xc}\right]}{2w^2}\right) \tag{1}$$

DOI: 10.13009/EUCASS2019-258

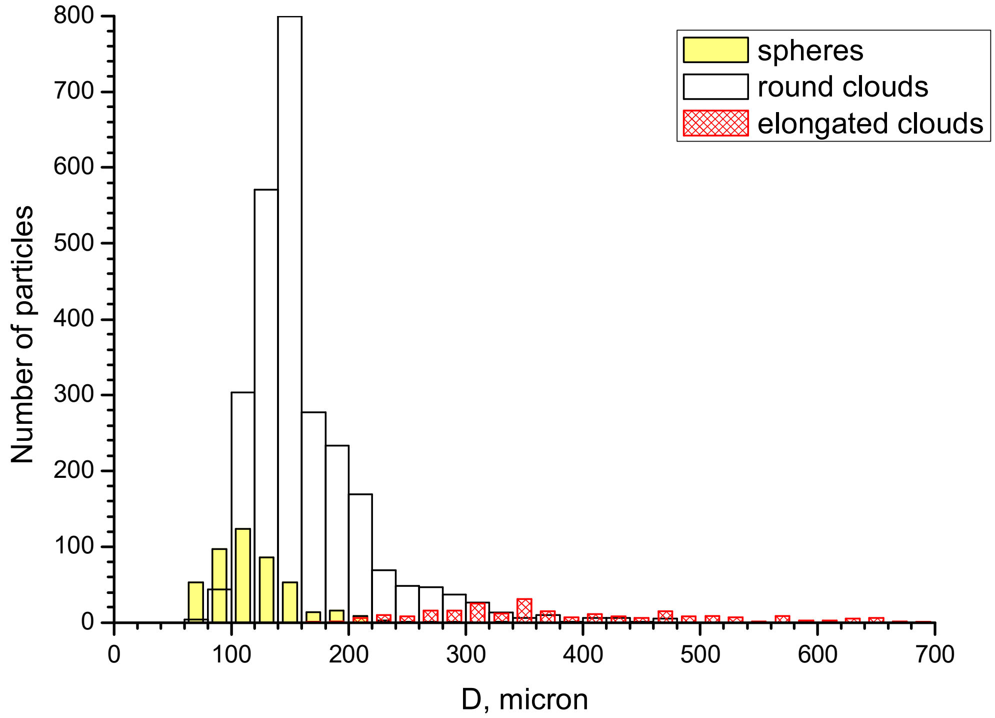

Figure 7: Size distribution of particles by number for the main morphological types (compact spheres, round, and elongated clouds of nanoparticles) within the range 60-700 µm. Counting histograms are normalized to the number of burning mother particles-sources equal to five

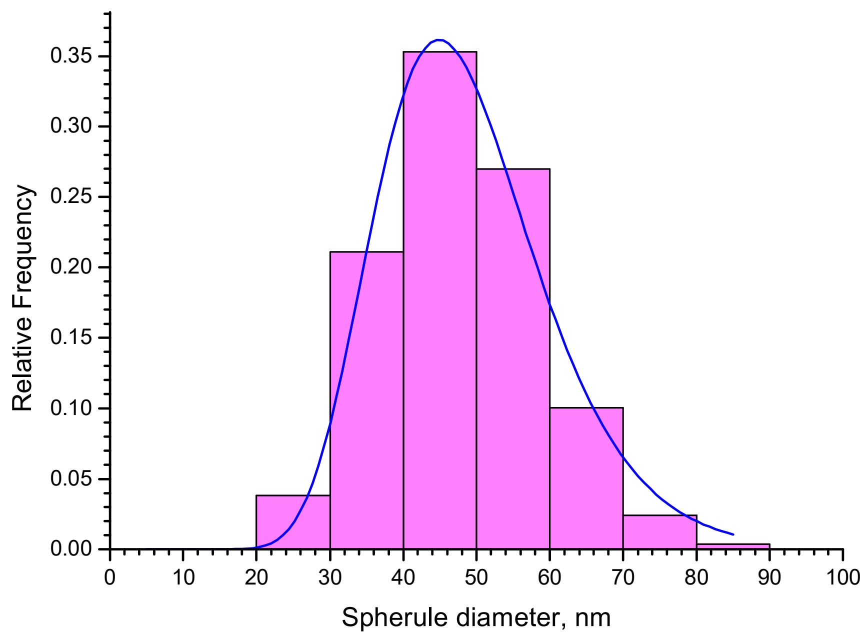

Figure 8: Size-distribution of a relative frequency of the number of spherules

DOI: 10.13009/EUCASS2019-258

4. Conclusions and future plans

The condensed combustion products of titanium particles with a diameter of 300-500 µm, burning in free fall in air have been studied in detail for the first time. For the particles of all morphological types, we have performed the particle-size analyses and approximated the distribution functions by log-normal law. The nanosized combustion products are represented by aerogel objects, consisting of spherules with a median diameter of 48 nm. The shape and size of aerogel objects reflect the life history of the particles that have generated them. The most common (in number) combustion products are the round aerogel clouds. In terms of one mother particle with a diameter of 437 µm, the number of clouds, exceeding 60 µm, amounts to 2676 (799 clouds are of a mode size of 150 µm) plus 13499 clouds smaller than 60 µm. The number of dense, spherical particles is one and a half times less. The number of elongated clouds is ten times less. However, these can reach 15 mm in length.
In the future, we are going to compare the quantitative characteristics of the combustion products of mother particles of different, initial diameters, and to determine the effective density of aerogel objects.

Acknowledgements

The work was supported by the Russian Foundation for Fundamental Research (project № 19-03-00294).
The authors are grateful to Karasev V. V. and Zhitnitskaya O.N. for their assistance in granulometric analyses.

References

[1] Glotov O.G., Zarko V.E. 2016. Formation of Nanosized Products in Combustion of Metal Particles. In: *Energetic Nanomaterials: Synthesis, Characterization, and Application*. Elsevier. 285-321.
[2] Yu J. 2016. Combustion behaviors and flame microstructures of micro- and nano-titanium dust explosions. *Fuel*. 181: 785–792.
[3] Gao W., Zhanga X., Zhang D., Peng Q., Zhangd Q., Dobashi R. 2017. Flame propagation behaviours in nano-metal dust explosions. *Powder Technology*. 321: 154–162.
[4] Weiser V., Neutz J., Eisenreich N., Roth E., Schneider H., Kelzenberg S. 2005. Development and characterization of pyrotechnic compositions as counter measures against toxic clouds. In. *36th Int. Annual Conf. of ICT & 32nd Int. Pyrotechnics Seminar. Energetic Materials: Performance and Safety*. 102-1–102-12.
[5] Kelzenberg S., Weiser V., Roth E., Schulz O., Eisenreich N. 2009. Flame Investigation of Burning Titanium Powder. In *ECM 2009 – European Combustion Meeting*. 1–6.
[6] Poletaev N.I., Zolotko A.N., Doroshenko Y.A., al E. 2011. Degree of dispersion of metal combustion products in a laminar dust flame. *Combustion, Explosion and Shock Waves*. 47: 153-165.
[7] Zakharov R.S., Glotov O.G. 2007. Combustion characteristics of pyrotechnic compositions containing powdered Ti. *Bulletin of Novosibirsk State University, Physics series*. 2: 32-40. [in Russian]
[8] Glotov O.G. 2013. Combustion of spherical titanium agglomerates in air. I. Experimental approach. *Combustion, Explosion, and Shock Waves*. 49: 299–306.
[9] Glotov O.G. 2013. Combustion of spherical titanium agglomerates in air. II. Experimental results. *Combustion, Explosion, and Shock Waves*. 49: 307–319.
[10] Glotov O.G., Surodin G.S., Baklanov A.M. 2019. Combustion of Spherical Titanium Agglomerates in Air. III. Movement of Agglomerates and the Effect of Airflow Velocity on Nanosized Combustion Products and Burning Time. *Combustion, Explosion and Shock Waves*. 55: 43-55.
[11] Glotov O.G. 2019. Ignition and combustion of titanium particles. Experimental methods and results. *Physics-Uspekhi*. 62: 131-165.
[12] Glotov O.G., Belousova N.S., Surodin G.S., Zarko V.E. 2018. Combustion characteristics of coarse titanium particles in air. In *49th International Annual Conference of the Fraunhofer ICT Energetic materials. Synthesis, Processing, Performance*. 111-1–111-14.
[13] Glotov O.G., Belousova N.S., Surodin G.S., Zarko V.E. 2018. Combustion characteristics of coarse titanium particles in air. In *XIV International Workshop "HEMs-2018"*. 35-38.
[14] Glotov O.G., Zhukov V.A. 2008. The evolution of 100-µm aluminum agglomerates and initially continuous aluminum particles in the flame of a model solid propellant. II. Results. *Combustion, Explosion, and Shock Waves*. 44: 671-680.
[15] Karasev V.V., Onischuk A.A., Khromova S.A., Glotov O.G., Zarko V.E., Pilyugina E.A., Tsai C.J. 2006. Formation of Metal Oxide Nanoparticles in Combustion of Titanium and Aluminum Droplets. *Combustion, Explosion, and Shock Waves*. 42: 649-662.